Radioecological assessment and radiometric dating of sediment cores from dynamic sedimentary systems of Pra and Volta estuaries (Ghana) along the Equatorial Atlantic

E. Klubi [a], J.M. Abril [b, *], E. Nyarko [a], A. Laissaoui [c], M. Benmansour [c]

[a] Department of Marine and Fisheries Sciences, University of Ghana, Legon, Spain
[b] Departamento de Física Aplicada I, ETSIA, Universidad de Sevilla, Spain
[c] Centre National des l'Energie, des Sciences et des Techniques Nucleaires-CNESTEN, Rabat, Morocco

Keywords:
Volta estuary
Pra estuary
^{210}Pb dating
Dynamic sedimentary systems
TERESA model
ERICA model

A B S T R A C T

The Volta and Pra estuaries (Ghana, West Africa) are dynamical sedimentary systems whose natural equilibrium is being affected by anthropogenic activities. This paper reports depth-distributions of ^{210}Pb, ^{226}Ra, ^{234}Th, ^{40}K, ^{228}Ra and ^{137}Cs for two sediment cores from these estuaries. Bulk densities were not steady-state and well correlated with ^{40}K ($p < 0.00005$). Unsupported ^{210}Pb profiles were incomplete, non-monotonic and showed large fluctuations. The assumptions involved in the common ^{210}Pb-based dating models were not meet in these dynamical scenarios, and the use of ^{137}Cs as a time-marker is difficult in Equatorial and South-Hemisphere countries due to its low fallout rates. Chronologies have been solved with the new ^{210}Pb-based TERESA model, which operates with varying but statistically correlated fluxes and sediment accumulation rates (SAR). The core from the Volta reflects the conditions prevailing after the construction of the Akosombo Dam, with a mean SAR of 1.05 ± 0.03 g cm^{-2}·y^{-1}, while a higher value of 2.73 ± 0.06 g cm^{-2}·y^{-1} was found in the Pra, affected by intense gold mining activities along its course. Radiological and radioecological assessments have been conducted by applying the UNSCEAR protocols and the ERICA model, respectively. The measured radionuclide concentrations do not pose any significant risk for the environment and human health.

1. Introduction

Sediment supply through river channels and/or longshore drifts are remarkable in building of coastal systems (Morton, 2003). The natural equilibrium may be distorted by a wide range of anthropogenic activities, affecting both the accretion/erosion rates and the concentration of some trace elements, such as radionuclides and heavy metals which could be harmful to the ecosystem. Accurate methods for establishing chronologies for recent-sediment cores are necessary for providing reliable estimates of sediment accumulation rate (SAR) and depositional processes, which are the keys for reconstructing past environmental conditions. Currently, radiometric dating is the only technique of general applicability that claims to provide an absolute age determination of deposited sediment (Carroll and Lerche, 2003).

Radiological studies have shown that radionuclides are ubiquitous as a result of their natural association with the earth crust and the atmosphere and the overall spread of some bomb-fallout radionuclides and others released in major nuclear accidents. They are easily transferred into the food web/chain through bioaccumulation and biomagnification which adversely impact human and ecosystems alike.

In the West Africa sub-region, exposure to radioactive materials from nuclear industries could be at its minimal due to absence of nuclear facility in the sub-region. However, there could be noticeable exposure through contaminated global sea circulation and oil exploration/exploitation and ship's ballast water and sediment at onshore and offshore platforms (Botwe et al., 2017). Open surface mining, tailing materials, dredge spoil, dredging of river channels as well as dipping and widening of drains may also lead to resuspension of deposited materials capable of increasing levels of radioactive concentration in aquatic ecosystems. In coastal aquatic

Abbreviations: TERESA, Time estimates from random entries of sediments and activities; SWI, sediment-water interface; SAR, sediment accumulation rate.

* Corresponding author. Departamento de Física Aplicada I, ETSIA, Universidad de Sevilla, Carretera de Utrera km 1, D.P. 41013 Sevilla, Spain.
E-mail address: jmabril@us.es (J.M. Abril).

ecosystems, estuaries are known to be effective traps of sediment due to convergence of residual flow at the bottom-water, tidal asymmetry, and reduction in fluvial energy as well as salinity induced sediment flocculation (Postma, 1967; Allen et al., 1980; Nichols et al., 1991; Lick and Huang, 1993; Woodruff et al., 2001). This implies that sediment from estuaries could be enriched with appreciable levels of radionuclides. Their radiological significances depend not only on concentrations but also on particularities of the ecosystem as well as the human interactions with the natural environment. These studies are of special interest due to the scarcity of field data in countries from Equatorial Africa, particularly in Ghana, as compared to other parts of the world.

The coastline of Ghana from Aflao (Ghana-Togo border) to New-Town (Ghana-Cote d'Ivoire border) is made of sandy beaches interspersed with rocky shores. The extreme ends of the coast are mostly sandy while the middle section is dominated by rocky shorest. The present study was conducted with sediment cores sampled in the Pra and the Volta estuaries which are located in the western and eastern coastal zones of Ghana respectively (Fig. 1). The cores were analyzed for the determination of the radionuclide depth distributions for supporting: i) a radiological assessment based on well-established protocols for estimating the cumulative dose received by humans through different exposure pathways; and ii) for a radioecological assessment of dose received by a wide group of biota species through the application of the ERICA tool (Fisher et al., 2013; Brown et al., 2016). The measurement of ^{210}Pb allowed the radiometric dating of the cores.

Goldberg (1963) first proposed the use of unsupported ^{210}Pb (^{210}Pb$_{exc}$ hereafter) for dating glacier ice. The method was then applied to lacustrine and marine sediments by Krishnaswamy et al. (1971) and Koide et al. (1972), respectively, and it has been widely used, with the development of new dating models and their application to a great diversity of sedimentary systems (e.g., see the review papers by Appleby, 2008; and Mabit et al., 2014). The ^{210}Pb-dating method is often complemented and/or validated with independent chronostratigraphic markers, mostly based on the depth distribution of some bomb-fallout radionuclides (mainly ^{137}Cs, ^{241}Am and $^{239+240}$Pu).

Sediment cores from dynamic sedimentary systems in equatorial regions represent a great challenge for the ^{210}Pb-dating method. The low radioactive fallout of ^{137}Cs in these regions makes it difficult to measure this isotope above the typical method detection limits; and the sedimentary conditions hardly meet the assumptions involved in most of the ^{210}Pb-based dating models (e.g., see Sánchez-Cabeza and Ruíz-Fernández, 2012). Thus, SAR, the initial activity concentration associated to the mass flow, and the resulting ^{210}Pb$_{exc}$ fluxes onto the sediment-water-interface (SWI) may all vary with time. Abril and Brunskill (2014), through a wider statistical analysis of varved sediment, show that ^{210}Pb$_{exc}$ fluxes were linearly related with SAR. More recently, Abril (2016) developed the TERESA model, which is based on the above statistical correlation. The model has been validated against data from synthetic cores and against real data from varved sediments, for which an independent chronology was available. The basic assumptions of this model can be met in the studied dynamic sedimentary systems of the Volta and Pra estuaries, in Ghana. Thus, results from the present study, obtained with the above referred new analytical methods, may be of great interest for those members of the international scientific community working with sediments from dynamical coastal and estuarine environments.

2. Material and methods

2.1. Site description

The Pra Estuary is located on a relative stable coast in the Shama District of Ghana's Western Region forming the lower section of the Pra River system (Fig. 1). The estuary is within a valley of less than 150 m above mean sea level. The habitat is mainly dominated by species of mangrove providing suitable substrates for crabs, fish and avifauna. It also provides water transport for peripheral communities while the extreme lower end is used as a fish landing site. The mangrove species (red mangroves) are mostly harvested for fish smoking by fishmongers, a situation associated with coastal communities in Ghana (Tanner et al., 2014). The upland section of the river serves as sites for quarries.

The Volta Estuary is located in Ada-Foah in the Dangbe East District of the Ghana's Greater-Accra Region (Fig. 1). It is situated on low lying plains of the Volta Delta. The coastline of the delta and its contiguous coasts could be described as episodic sand dunes deposited over time which is currently eroding. The estuary is one of the biggest estuaries along the coast of Ghana with multiple

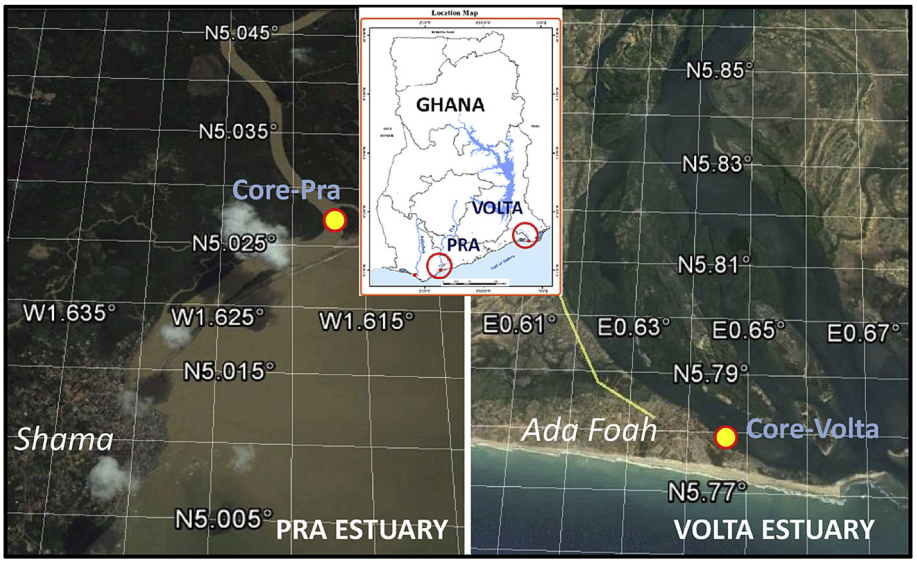

Fig. 1. Map of Ghana showing the sampling sites in the Pra and Volta estuaries (images from Google Earth).

islands inhabited by local indigenes. Coconut and mangrove plants dominate the vegetation cover at the estuary, while the bottom floor provides suitable substrate for the popular *Galatea paradoxa*, a mollusc-bivalve, as well as other benthic fauna such as blue swimming crabs and tiger shrimps (Adjei-Boateng et al., 2012). The estuary also provides water transport for the communities and part of the Keta Municipal Districts in the Volta region of Ghana. There is also dry dock facility constructed by the Volta River Authority of Ghana for maintenance of its vessels that ply the lower section of the Volta River. The Volta Estuary also serves as tourist site for many visitors engaging in swimming and boating in the estuary.

2.2. Sampling and radionuclide analyses

Two sediment cores of about 55 cm length each were sampled from the Volta (0.6418° E, 5.7819°N) and Pra (1.6166° W, 5.0278°N) estuaries (Fig. 1) on January 7th and May 4th, 2012, respectively. They were sampled at 0.9 m water depth during low tide using a UWITEC corer of 8.7 cm inner diameter. The cores were carefully corked at both ends, vertical positioned in the core holder with SWI facing upwards, and conveyed into the laboratory. Selection of sampling locations focused in the highest deposition areas of the estuaries by observing the bent and flow of the water masses.

At the laboratory the water retained at the SWI of the core was carefully siphoned after settling and the entire core was sectioned into 2 cm thickness using a core slicer. About 0.5 cm of the outer area of each slice was discarded to minimize cross contamination. Wet and dry masses were determined before and after drying the samples at a constant temperature of 80 °C for 48 h in a drying oven. The bulk density of each slice was calculated using the dry weight fraction approach while equating the particle density of mineral soil as 2.5 g cm^{-3} (Velinsky et al., 2011). The samples were then grounded to fine powder using electronic grinder and homogenized.

For determination of total ^{210}Pb activities, about 0.5 g of each homogenized sample was spiked with 50 μl of ^{209}Po yield tracer (certified specific activity of 0.357 ± 0.011 Bq.g^{-1}) and digested in 100 ml Teflon beakers using a mixture of concentrated nitric, hydrochloric and hydrofluoric acids (3:1:1 ratio respectively). The mixture was heated at 80 °C in a fume hood with addition of few drops of hydrogen peroxide to achieve complete digestion of associated organic matter. The resultant solution was further treated with HCl-boric acid solution to dryness to remove the remaining hydrofluoric acid and then diluted with 0.5M HCl solution. The solution was filtered into 100 ml beaker and completed to a total volume of 80 ml with 0.5M HCl solution. The possible interferences of iron oxides with polonium were minimized by addition of ascorbic acid prior to self-deposition. Self-deposition of polonium isotopes was achieved through the introduction of one-sided-blanked (using adhesive cellulose tape) silver disc on a hot plate at 80 °C with continuous stirring for 4.5 h. The discs were removed from the solutions, washed with ethanol, dried and then counted for about 24 h in a calibrated ORTEC alpha-spectrometer interfaced with Maestro™ data acquisition software. Activity concentrations of ^{210}Po were computed using gross counts of each radionuclide isotopes and the chemical recoveries were within 40–95%.

The activity concentrations of gamma emitting radio-isotopes of the homogenized samples were estimated using HPGe detector (p-type) gamma spectrometer with resolution of 2 keV and a relative efficiency of 30% at 1332 keV. The detector was calibrated for energy and efficiency using a multi-gamma certified source containing a mixture of gamma emitting radionuclides. The samples were sealed in pre-defined geometry vials to prevent escape of ^{222}Rn, and stored for 21 days to establish secular equilibrium between ^{226}Ra, ^{214}Bi and ^{214}Pb. The sealed samples were counted for about 24 h each, and radionuclide activities were scanned determined from the net peak areas of 609.3 keV for ^{214}Bi, 351.9 keV for ^{214}Pb, 911.3 keV for ^{228}Ac, 238.6 keV for ^{212}Pb, 63.35 keV for ^{234}Th, 1460 keV for ^{40}K and 661.3 keV for ^{137}Cs. Specific activities of ^{226}Ra were estimated through its progeny radionuclides (^{214}Bi and ^{214}Pb). For radionuclides from the ^{232}Th series, ^{228}Ra was estimated through ^{228}Ac, and ^{228}Th through ^{212}Pb. The analytical procedure was checked using reference material (IAEA-327). The relative differences between measured and certified values were less than 10% for all radionuclides. Excess or unsupported ^{210}Pb activity concentrations were determined on a level by level basis by subtracting the activity concentrations of supported ^{210}Pb (^{226}Ra) from the total ^{210}Pb activity concentrations.

2.3. Radiological and radioecological risk assessments

Dredged sediments may be disposed of on land, or used for building or for other purposes, which can potentially cause some radiological effects. Five radiological hazard indices were estimated using established formulae for radiation dose to human as a result of the exposure to sediment materials (e.g., see Botwe et al., 2017); [1] total absorbed dose rate in air (D), [2] radium equivalent activity (Ra_{eq}), [3] external hazard index (H_{ex}), [4] annual gonadal dose equivalent ($AGDE$) and [5] annual effective dose equivalent ($AEDE$).

The D is the rate of exposure to gamma radiation in air at 1 m above the ground due to the activities of ^{226}Ra, ^{232}Th and ^{40}K in the sediment material; Ra_{eq} is the weighted summation of the activity concentrations of ^{226}Ra, ^{232}Th and ^{40}K in the sediment material; H_{ex} is a measure of the indoor radiation dose due to external gamma radiation exposure to natural radionuclides in building materials.

$$D\left(\mathrm{nGy\cdot h^{-1}}\right) = 0.462A_{Ra} + 0.604A_{\mathrm{Th}} + 0.0417A_K \quad (1)$$

$$Ra_{eq}\left(\mathrm{Bq\cdot kg^{-1}}\right) = A_{\mathrm{Ra}} + 1.43A_{\mathrm{Th}} + 0.077A_{\mathrm{K}} \quad (2)$$

$$H_{ex} = (A_{\mathrm{Ra}}/370) + A_{\mathrm{Th}}/259 + A_K/4810 \quad (3)$$

$$AGDE\left(\mu\mathrm{Sv\cdot y^{-1}}\right) = 3.09A_{\mathrm{Ra}} + 4.18A_{Th} + 0.314A_{\mathrm{K}} \quad (4)$$

$$AEDE\left((\mu\mathrm{Sv\cdot y^{-1}}\right) = D\left(\mathrm{nGy\cdot h^{-1}}\right) \times 8760\ \mathrm{h} \times 0.2 \times 0.7\ \mu\mathrm{Sv\cdot Gy.y^{-1}} \times 10^{-3} \quad (5)$$

The radiological protection framework based on human protection has been extended to the radioecological risk assessment through the development of The ERICA Integrated Approach [ERICA-Tool] (ICRP, 2008; Larsson, 2008). The key components are: concentration ratios, CR (i.e., ratio of activity concentration in the whole body of an organism to that in media) for water or soil; distribution coefficients, K_ds, (i.e., ratio of activity concentration in sediment to that in water) and dose conversion coefficients, DCCs (i.e., dose rate per unit activity concentration in the organism or media). The ERICA-tool has a wider data base on wildlife and media (terrestrial, freshwater, marine and estuaries) as well as natural and man-made radionuclides. It operates on three tier levels and also allows the addition of organisms and radioisotopes of interest to the default data base (Brown et al., 2008, 2016).

Tier 2 of *vz.* 1.2.1 of ERICA-tool was used to estimate activity concentrations of five (^{210}Pb, ^{226}Ra, ^{232}Th, ^{238}U and ^{137}Cs) selected radionuclides in water and in eleven selected biota (*benthic fish, mollusc-bivalve, crustaceans, polychaete worm, vascular plant, zooplankton, bird, mammal, pelagic fish, phytoplankton and reptiles*)

using (as the worst scenario) the highest radioactivity concentration in the 0–10 cm sediment layer of the Volta and Pra cores for the selected radionuclides. The derived activity concentrations were then further processed by the ERICA-tool by selecting defined occupancy factor(s) of each biota as well as applying a default uncertainty factor of 3.0 to ensure that there will be less than 5% probability of computed dose rate exceeding the screening dose rate. Default weighting factor of 10 was also selected for alpha, 1.0 for beta/gamma and 3 for low beta radiation to account for differences in magnitude of dose rate of each radionuclide to the selected biota (Schmid and Schrader, 2007; Brown et al., 2016).

The plausible bioaccumulation of radioactive substances by filter feeders such as *Galatea paradoxa*, *crustacean* and *detritivore* (*benthic fish*) were considered as a pathway to humans. Hence, the radioactive concentrations derived from ERICA for these biota classes were used as a proxy for the calculation of dose to human due to their consumption. An overall consumption rate of fish products of 25 kg yr^{-1} (Rurangwa et al., 2015) was considered as representative for the general population of Ghana. This has been equally distributed among the k biota classes to get the ingestion rate of each one, IR_k. The 50 year committed effective dose, E_{ing} (given in Sv), is then (UNSCEAR, 2008):

$$E_{ing} = \sum_{k,j} C_{k,j} e_{j,ing} IR_k, \quad (6)$$

where j refers to radionuclides and k to the type of food; $C_{k,j}$ is the concentration ($Bq \cdot kg^{-1}$) and $e_{j,ing}$ is the coefficient from conversion from intake to committed effective dose integrated for 50 years for adults (UNSCEAR, 2008).

2.4. TERESA model

In the Results and Discussion section, it will be shown that the conditions for the application of the standard ^{210}Pb-based dating models CRS, CIC and CF-CS are not met. Indeed, the bulk density profiles are not steady-state, and most likely both, fluxes and SAR are highly variable with time. This discard the application of all the families of models based on the assumption of steady-state conditions (Robbins, 1978). The SIT model (Caroll and Lerche, 2003) claims its ability for handling these complex situations, but as demonstrated by Abril (2015), the model fundamentals lack of a sound physical basis. Moreover, in the above reference this author showed that the $^{210}Pb_{exc}$ vs. mass depth profiles do not contain enough information as to extract a unique chronology when both, $^{210}Pb_{exc}$ fluxes and SAR independently vary with time. Restrictive assumptions are needed to develop a suitable dating tool. A statistical correlation between fluxes and SAR seems to be a quite general rule (Abril and Brunskill, 2014). This allowed for the development of a new ^{210}Pb-based dating tool by using such a statistical correlation: the TERESA model (time estimates from random entries of sediments and activities). The model's fundamentals and validation against synthetic cores and real data from varved sediments (for which an independent chronology was available) have been published in the work by Abril (2016). Thus, only a brief summary is explained here.

The model stands on the following set of assumptions: i) $^{210}Pb_{exc}$ behaves as a particle-associated tracer and new inputs are ideally deposited at the SWI over the previously existing material; ii) there is no post-depositional redistribution; iii) continuity of the sequence (i.e., no missing of sediment layers by erosion); iv) $^{210}Pb_{exc}$ fluxes are governed by 'horizontal inputs', and thus there is a statistical correlation between fluxes and SAR (Abril and Brunskill, 2014).

For a sediment core which has been sectioned into N slices of mass thickness Δm_i (i = 1,2, … N), each one has an associated age interval ΔT_i, a mean SAR value w_i, and an associated initial activity concentration $A_{0,i}$(the one encountered when that sediment slice was at the SWI). TERESA model operates with SAR and initial activities distributions of $w_i$and $A_{0,i}$which closely follow normal distributions around their arithmetic mean values,$\overline{w}$and$\overline{A}_0$, with standard deviations $\sigma_w$andσ_A, respectively, while $s_w$and s_A are their corresponding normalized values. Provided a first estimation of $\overline{w}$, $\overline{A}_0$, $\sigma_w$and σ_A, the model then generates independent random distributions with values for w_i and $A_{0,i}$; and an intelligent algorithm solves their best arrangement downcore to fit the experimental $^{210}Pb_{exc}$ vs. mass depth profile, in this way solutions for the chronological line and for the histories of SAR and fluxes are resolved (Abril, 2016). As the result depends on the first estimation of$\overline{w}$,$\overline{A}_0$, $\sigma_w$and σ_A, the model applies a mapping technique by iterating the whole process for each parameter varying over a wide range. The error function, Q^2, measures the overall quality of the fit for each individual run of the model:

$$Q^2 = \sum_{i=1}^{N} \frac{(A_{th,i} - A_i)^2}{\sigma_i^2};$$

where A_i and σ_i are, respectively, the measured value and the analytical error of the activity concentration at the slice with index i, and $A_{th,i}$ is the corresponding value estimated by the model. Parametric maps of a χ-function ($\chi^2 = Q^2/f$; with f the number of degrees of freedom) serve to find out the best solution and to support error estimates (Abril, 2016). Optionally, the model's answers can be better constrained through the use of time markers, when available.

3. Results and discussion

3.1. Bulk densities and radionuclide concentrations in sediment cores

Fig. 2 plots the measured bulk density vs. actual depths for the cores from the Volta and Pra Estuaries; and Tables 1 and 2 report the cumulative mass depths and the measured specific activities for ^{234}Th, ^{210}Pb, ^{226}Ra, ^{40}K, ^{228}Ra and ^{137}Cs. Radionuclides from the ^{232}Th series were found in secular equilibrium (within the involved counting uncertainties) and thus, only data for ^{228}Ra are reported.

Early compaction is the result of the gravity-driven displacement of water-pore spaces by solids in the top sediment layers

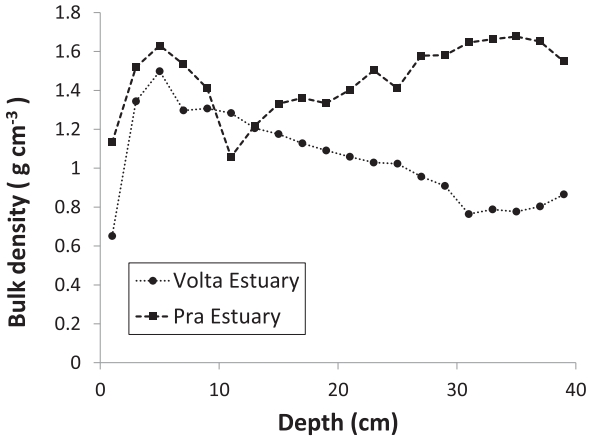

Fig. 2. Measured bulk density vs. actual depths for the cores from the Volta and Pra estuaries.

Table 1
Mass depth (m) and radionuclide specific activities for ^{234}Th, ^{210}Pb, ^{226}Ra, ^{40}K, ^{228}Ra and ^{137}Cs in the sediment core from the Volta Estuary.

Depth (cm)	m (g cm^{-2})	Radionuclide specific activity (Bq·kg^{-1})																		
		^{234}Th			^{210}Pb			^{226}Ra			^{40}K			^{228}Ra			^{137}Cs		
0–2	0.62	69	±	25	87.0	±	6.2	18.3	±	3.2	319	±	25	30.5	±	3.4	BDL		
2–4	2.54	63	±	20	25.2	±	2.6	13.0	±	2.3	236	±	19	23.3	±	2.6	BDL		
4–6	5.29	26	±	16	20.1	±	2.3	11.9	±	1.8	229	±	16	13.5	±	1.9	BDL		
6–8	8.00	21	±	16	32.3	±	2.8	12.2	±	2.0	236	±	17	22.4	±	2.3	BDL		
8–10	10.51	BDL			19.9	±	1.6	16.0	±	2.5	238	±	19	24.6	±	5.5	BDL		
10–12	13.02	BDL			25.9	±	2.2	14.5	±	2.3	253	±	18	24.4	±	2.4	BDL		
12–14	15.42	26	±	21	32.9	±	2.8	18.4	±	2.7	291	±	22	27.4	±	3.0	1.6	±	1.1
14–16	17.71	27	±	17	37.5	±	3.3	17.4	±	2.4	296	±	20	31.8	±	2.9	1.2	±	0.6
16–18	19.93	BDL			34.5	±	2.9	19.6	±	2.7	306	±	22	34.2	±	3.1	2.0	±	0.7
18–20	22.06	65	±	25	45.6	±	3.6	25.3	±	3.4	281	±	22	30.3	±	3.2	BDL		
20–22	24.12	BDL			36.5	±	3.4	17.2	±	2.3	284	±	19	30.7	±	2.6	0.8	±	0.6
22–24	26.12	BDL			38.6	±	3.2	20.0	±	2.9	320	±	23	40.4	±	3.5	BDL		
24–26	28.09	44	±	11	33.9	±	2.8	21.2	±	2.5	308	±	21	28.7	±	2.7	BDL		
26–28	29.99	34	±	18	36.2	±	2.9	25.4	±	2.9	343	±	22	38.2	±	3.0	BDL		
28–30	31.77	BDL			45.0	±	3.7	25.5	±	2.7	373	±	23	33.6	±	2.9	BDL		
30–32	33.37	29	±	21	30.8	±	2.1	17.8	±	2.7	377	±	25	41.2	±	4.0	BDL		
32–34	34.84	BDL			36.9	±	3.0	19.3	±	2.9	377	±	26	38.5	±	3.5	BDL		
34–36	36.33	N.R.			44.5	±	3.7	26.0	±	2.9	N.R.			N.R.			N.R.		
36–38	37.84	N.R.			40.8	±	3.5	22.7	±	2.9	N.R.			N.R.			N.R.		
38–40	39.43	BDL			44.3	±	3.5	24.1	±	3.6	337	±	25	33.9	±	3.5	BDL		

Cumulative mass depth, m, is referred to the mid-point interval of each sediment slice.
BDL: Below the detection limit (0.6 Bq·kg^{-1} for ^{137}Cs and 16 Bq·kg^{-1} for ^{234}Th).
N.R.; not reported.

Table 2
Mass depth (m) and radionuclide specific activities for ^{234}Th, ^{210}Pb, ^{226}Ra, ^{40}K, ^{228}Ra and ^{137}Cs in the sediment core from the Pra Estuary.

Depth (cm)	m (g cm^{-2})	Radionuclide specific activity (Bq·kg^{-1})																		
		^{234}Th			^{210}Pb			^{226}Ra			^{40}K			^{228}Ra			^{137}Cs		
0–2	1.09	44	±	24	25.1	±	2.4	24.4	±	4.0	218	±	21	36.2	±	3.3	BDL		
2–4	3.65	29	±	27	26.7	±	2.8	13.3	±	2.7	141	±	15	23.4	±	2.5	BDL		
4–6	6.72	37	±	19	26.9	±	2.9	14.9	±	2.9	143	±	15	27.5	±	2.7	BDL		
6–8	9.80	BDL			24.2	±	2.5	22.9	±	3.2	180	±	17	31.7	±	2.8	BDL		
8–10	12.66	45	±	20	37.6	±	3.4	25.6	±	3.6	249	±	20	45.9	±	6.5	BDL		
10–12	15.04	BDL			58.2	±	5.5	25.7	±	3.8	287	±	22	39.4	±	3.4	BDL		
12–14	17.23	32	±	19	52.5	±	4.8	34.2	±	4.1	308	±	23	42.1	±	3.5	BDL		
14–16	19.69	39	±	20	43.8	±	3.7	23.7	±	4.1	271	±	23	34.8	±	3.5	BDL		
16–18	22.30	35	±	22	37.3	±	1.4	21.4	±	4.3	245	±	20	37.1	±	3.7	BDL		
18–20	24.90	36	±	24	43.7	±	2.7	24.1	±	4.5	274	±	24	36.0	±	3.7	1.4	±	1.1
20–22	27.55	BDL			37.9	±	3.8	27.5	±	4.2	260	±	22	38.7	±	3.7	BDL		
22–24	30.37	19	±	16	37.2	±	3.4	20.9	±	4.1	162	±	20	28.2	±	3.1	BDL		
24–26	33.20	BDL			22.9	±	3.1	13.3	±	2.4	101	±	12	20.0	±	2.1	BDL		
26–28	36.10	BDL			40.7	±	1.9	18.0	±	2.8	131	±	11	26.1	±	2.4	BDL		
28–30	39.18	BDL			30.3	±	2.1	13.5	±	2.5	163	±	12	24.8	±	2.3	BDL		
30–32	42.32	28	±	12	25.2	±	3.5	15.7	±	2.5	146	±	16	25.6	±	2.4	BDL		
32–34	45.55	43	±	22	18.2	±	2.6	13.0	±	3.1	75	±	15	23.0	±	2.5	BDL		
34–36	48.82	33	±	15	21.2	±	2.2	10.2	±	3.0	97	±	15	17.0	±	2.4	BDL		
36–38	52.06	BDL			16.3	±	1.8	15.6	±	2.5	120	±	13	21.6	±	2.1	BDL		
38–40	55.18	BDL			40.2	±	2.6	13.2	±	2.5	145	±	14	27.1	±	2.7	BDL		

Cumulative mass depth. m. is referred to the mid-point interval of each sediment slice.
BDL: Below the detection limit (0.6 Bq·kg^{-1} for ^{137}Cs and 16 Bq·kg^{-1} for ^{234}Th).

(Abril, 2003, 2011). The steady-state profiles of bulk density vs. depth follow an exponential saturation-type function. But this is not the situation observed in the studied cores. In the core from the Volta Estuary, after a sharp increase in the 0–6 cm depth interval, bulk density monotonically decreases until 30 cm depth. In the Pra core, bulk density shows a clearly anomalous behavior in the 0–12 cm interval, with intermediate relative maxima. In both cases the overall high values of bulk density (1.05 ± 0.23 g cm^{-3} and 1.46 ± 0.18 g cm^{-3} for the Volta and Pra estuaries, respectively) imply low water contents, and they are generally associated with a high fraction of coarse material (Keller and Häkansson, 2010).

Granulometric analysis in twin cores (sampled at the same time and place) were carried out by Mahu (2014), reporting high sand contents (40%, 50% in average for the Pra and Volta cores) and with a very large variability (e.g. a range from 4% to 65% was found for the Pra core). Thus, data on bulk densities are suggesting highly dynamics and non-steady sedimentary conditions at the two studied sites.

Previous radioecological studies in the coastal marine environment of Ghana are scarce, and focused on sediments from beaches (Amekudzie et al., 2011; Nyarko et al., 2011), estuaries (Mahu et al., 2016), harbors (Botwe et al., 2017) and produce water from offshore oil fields (Kpeglo et al., 2016). The ^{226}Ra specific activities measured in the Volta (mean 19.3, range 11.9–26.0, in Bq·kg^{-1}) and Pra (mean 19.6, range 10.2–34.2, in Bq·kg^{-1}) cores (Tables 1 and 2) are within the normal range found in sediment cores, and particularly they compare well with the ones reported by Botwe et al. (2017) in the Tema Harbor in Ghana (10–20 Bq·kg^{-1}), or with those reported

by Laissaoui et al. (2013) for the Sebou Estuary in Morocco (17–19 $Bq \cdot kg^{-1}$).

The specific activities of ^{228}Ra and ^{40}K reported in Tables 1 and 2 also compare well with the values reported in the above cited references. Due to the low ^{137}Cs fallout in equatorial regions, this isotope is difficult to solve from the method detection limit. When measured, its specific activity was below 2.0 $Bq \cdot kg^{-1}$. These results are consistent with the concentrations below 2.3 $Bq \cdot kg^{-1}$ reported for the Tema Harbour, in Ghana (Botwe et al., 2017). The ^{210}Pb specific activities measured at the top sediment slices were much lower than those found in the Tema Harbour (range 110–310 $Bq \cdot kg^{-1}$; Botwe et al., 2017), but comparable to those reported for the Sebou Estuary (39–55 $Bq \cdot kg^{-1}$; Laissaoui et al., 2013) and to the ones below 125 $Bq \cdot kg^{-1}$ reported by Mahu et al. (2016) for the Volta Estuary. The lower values found in the estuarine environments, when compared with the Tema Harbour, are likely due to a coarser granulometry (Abril and Fraga, 1996).

The gamma detector used in this work had a high background level at low energies. Consequently the reported specific activities for ^{234}Th (which should be in secular equilibrium with ^{238}U after the 1.6 y elapsed time between sampling and measurements) were affected by large statistical counting uncertainties. The obtained activities for ^{234}Th ranged between 21 and 69 $Bq.kg^{-1}$ and compare well with the range 21–47 $Bq \cdot kg^{-1}$ reported for the Tema Harbor (Botwe et al., 2017).

It is quite noticeable the statistical correlation found between ^{40}K specific activity and the bulk density, which holds for both cores (Fig. 3, $R^2 = 0.81$, $p < 0.00005$). Although it has been reported that bulk densities are governed, among other factors, by the granulometry of the substrate (Keller and Häkansson, 2010), and how the particle size affects the concentration of some radionuclide (Abril and Fraga, 1996), a fully quantitative explanation of this correlation cannot be supported from the available data. The correlation also holds for the two Radium isotopes, as shown in Fig. 4 with their normalized depth distributions compared against the ^{40}K data. From this figure it is also apparent that the isotopic ratio $^{228}Ra/^{226}Ra$ remains essentially constant downcore (1.6 ± 0.3 and 1.6 ± 0.2 for the cores from the Volta and Pra estuaries, respectively -mean and standard deviation).

3.2. Radiological and radioecological assessments

Table 3 reports the calculated hazard indices (Eqs. (1)–(5)) for the Volta and Pra sediment cores using the worst scenario (e.g., the highest activity concentrations in the 0–10 cm layer of the sediment cores) as well as comparing them with other reported hazard

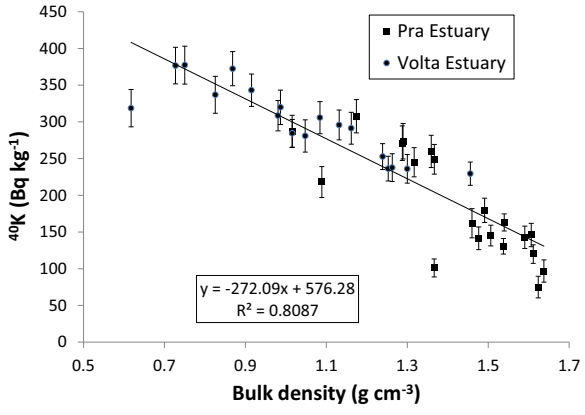

Fig. 3. Measured ^{40}K activity concentrations versus bulk density for the cores from the Volta and Pra estuaries.

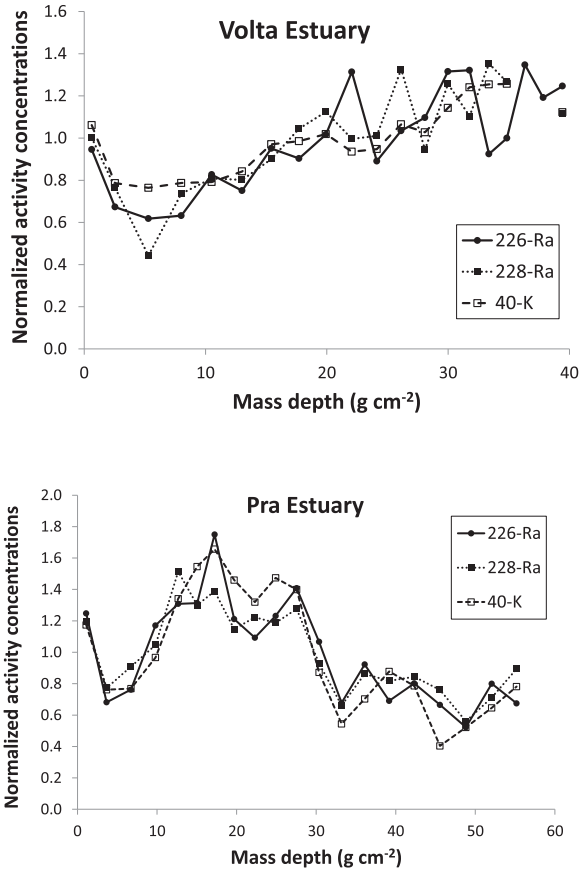

Fig. 4. Normalized (to their arithmetic mean values) depth-distributions of ^{226}Ra, ^{228}Ra and ^{40}K for the cores from the Volta and Pra estuaries.

indices from other parts of the world. Comparatively, all the hazard indices estimated were in close approximation, with Pra sediment recording slightly higher values than the Volta cores except for H_{ex} where they are par. The values of these indexes were below the world recommended dose (see Table 3) and therefore, they do not pose any radiological risk to human health.

Table 4 reports the radioactivity concentrations in reference organisms after applying ERICA model with its default parameter values and with the highest values of the radionuclide concentrations found in the top 0–10 cm layer of the cores from the Volta and the Pra estuaries. The ERICA-derived total dose rates to the reference organisms (from data in Table 4) are summarized in Tables S–1 (in Electronic Supplementary Material, ESM). The total dose rates to all the reference organisms fell below the screening dose rate of 400 $\mu Gy\ h^{-1}$, and therefore unlikely to cause harmful effects (UNSCEAR, 2000).

The ERICA-derived activity concentrations in *mollusc-bivalve* (*Galatea paradoxa*), *crustacean* and *benthic fish* (Table 4) due to the set of studied radionuclides served to estimate (by Eq. 6) the committed effective dose integrated for 50 years for adults by using the conversion coefficients recommended by UNSCEAR (2008) and the overall consumption rate of 25 $kg\ y^{-1}$ (see Methods section). It resulted of $1.2 \cdot 10^{-4}$ Sv and $5.3 \cdot 10^{-5}$ Sv for the Volta and Pra estuaries, respectively. These values are far from producing any harmful effects (UNSCEAR, 2008).

3.3. Radiometric dating with TERESA model

The $^{210}Pb_{exc}$ vs. mass depth profiles for cores from the Volta and

Table 3
Estimated *D*, Ra_{eq}, H_{ex}, *ADGE* and *AEDE* values for the Volta and Pra estuaries and sediments from other studies.

Estuaries	*D* ($nGy \cdot h^{-1}$)	Ra_{eq} ($Bq \cdot Kg^{-1}$)	*Hex*	*AGDE* ($\mu Sv \cdot y^{-1}$)	*AEDE* ($nGy \cdot h^{-1}$)	References
Volta	30	64	0.2	213	37	This study
Pra	33	72	0.2	233	41	This study
Average data of other studies						
Tema Harbour, Ghana	39	83	0.2	273	47	Botwe et al., 2017
Caspian Sea, Iran	63	176	0.5	–	–	Abdi et al., 2009
Red Sea coast, Egypt	42	101	–	–	–	El Mamoney and Khater, 2004
Ghana Coast	77	9	0.5	–	0.1	Amekudzie et al., 2011
Recommended values	55[a,b]	89[a]	1.0[c]	300[c]	70[c]	

D (total absorbed dose rate in air); $\boldsymbol{Ra_{eq}}$ (Radium equivalent activity); $\boldsymbol{H_{ex}}$ (external hazard index); ***AGDE*** (Annual gonadal dose equivalent); ***AEDE*** (annual effective dose equivalent): [a]Kurnaz et al., 2006; [b]Abdi et al., 2009; [c]Xinwei et al., 2006; – not reported.

Table 4
Radionuclide specific activities[a] of the Volta and Pra cores and ERICA derived radionuclide specific activities in reference organisms.

Specific activity in sediment ($Bq \cdot kg^{-1}$)		Reference organisms (Bq·kg-1 fresh weight)										
		Benthic fish	*Mollusc- bivalve*	*Crustacean*	*Polychaete worm*	*Vascular plant*	*Zooplankton*	*Bird*	*Mammal*	*Pelagic fish*	*Phytoplankton*	*Reptile*
Volta Estuary												
^{210}Pb	87.0	10.78	2.06	6.86	13.07	0.33	5.55	6.21	6.21	10.78	156.78	6.21
^{226}Ra	18.3	0.48	0.22	0.29	0.48	0.31	0.28	0.56	0.56	0.48	3.92	0.56
^{232}Th	33.5	0.01	0.01	0.16	0.01	0.02	0.03	0.01	0.01	0.01	3.07	0.01
^{238}U	61.3	0.20	0.74	0.08	22.8	5.41	0.09	0.20	0.2	0.20	5.02	0.20
^{137}Cs	2.0	0.02	0.01	0.01	0.03	0.00	0.02	0.09	0.04	0.02	0.00	0.09
Pra Estuary												
^{210}Pb	37.6	4.66	0.89	2.97	5.65	0.14	2.40	2.69	2.69	4.66	67.84	2.69
^{226}Ra	25.6	0.67	0.31	0.41	0.67	0.43	0.39	0.79	0.79	0.67	5.49	0.79
^{232}Th	33.7	0.01	0.01	0.16	0.01	0.02	0.03	0.01	0.01	0.01	3.09	0.01
^{238}U	45.0	0.15	0.54	0.06	16.76	3.97	0.06	0.15	0.15	0.15	3.69	0.15
^{137}Cs	1.4	0.01	0.01	0.01	0.02	0.00	0.02	0.06	0.03	0.01	0.00	0.06

Specific activities in sediments are reported y a dry weight basis.
[a] The reported values correspond to the highest specific activities found within the top 10 cm of the sediment core.

Pra estuaries are shown in Fig. 5. They show very large fluctuations and they do not follow a monotonic trend of decrease. Consequently, the conditions for the CF-CS model are not met, and the CIC model will produce age reversals. The activity concentrations in the deepest measured sediment layer are far from being null, and as the profiles do not follow any recognizable trend-line, then it is not possible a reliable estimate of the total $^{210}Pb_{exc}$ inventory. Furthermore, the scarce and non-accurate ^{137}Cs data do not allow any reliable identification of chronostratigraphic horizons. Consequently, the CRS model cannot be technically applied (independently of the reliability of the model assumptions for these scenarios). The fundamentals of these models can be seen, among others, in the work by Sánchez-Cabeza and Ruíz-Fernández (2012). Bulk density profiles (Fig. 2) fail to attain a steady-state, and most likely both, fluxes and SAR could be highly variable with time (Abril and Brunskill, 2014). This discard the application of all the families of models based on the assumption of steady-state conditions (Robbins, 1978); but the assumptions required for TERESA model (see Method Section) seem to be reliable for the studied sites.

As there are no available time-marks, the stand-alone version of the TERESA model has to be applied (Abril, 2016). Fig. 6 shows the computed maps for the χ function (see Method's section) in the $(\overline{A}_0,\overline{w})$ and (s_A,s_w) spaces. In the case of the Volta Estuary a single and well defined valley is encountered. The parameter values, with their associated fitting uncertainties are reported in Table 5. It is worth noting that due to the required large values for the normalized standard deviations, to avoid the generation of negative values or influencing points, lower threshold limits of $0.1\overline{A}_0$ and 0.2 $\overline{w}$have been imposed in all the calculations. This implies that the distributions of initial activity concentrations and SAR are not purely normal ones, but this does not contradict the fundamentals of TERESA model, since normal distributions are only a proxy to the distributions found in nature (see Abril and Brunskill, 2014). The computed $^{210}Pb_{exc}$ vs. mass depth profile is shown in Fig. 5 (panel 1), and it perfectly match the experimental data ($\chi = 0.29$).

The resulting chronology for the core from the Volta Estuary is reported in Fig. 7. The age of the oldest layer is 38 ± 1 y, that implies a time-averaged SAR value of 1.05 ± 0.03 g $cm^{-2} \cdot y^{-1}$. It is worth noting that the value reported in Table 5 (1.63 ± 0.01 g $cm^{-2} \cdot y^{-1}$) is the arithmetic mean of the values for the $N = 20$ sediment slices of the sediment (the one for which holds the statistical correlation shown by Abril and Brunskill, 2014). It has been shown (Ly, 1980) that after the construction of the Akosombo Dam (1961–1965) approximately 99.5% of the river drainage basin became blocked, and only a minor quantity of sand sediment derived from the low-lying areas of coastal plains below the dam continued to being supplied to the shoreline. This might led to severe erosion problems in the eastern coastal zone of Ghana. According to the chronology (Fig. 7) the deepest slice in the studied core is more recent than 1974; consequently, the core only can reflect the sedimentary conditions prevailing in the inner estuary after damming. It has been shown that ^{210}Pb-derived high-resolution SAR histories lack physical meaning (Abril, 2016), and only the major features of the chronological line may be linked to environmental changes. For the chronology of the Volta core (Fig. 7), a stepped change (high slopes in the age curve correspond to periods of low SAR) is observed around the date of the construction of the Kpong Dam (1982) and the severe draught of 1983. Relative low SAR values are also encountered for the period 2000–2008. No abnormal weather conditions have been recorded for this date interval, so this feature,

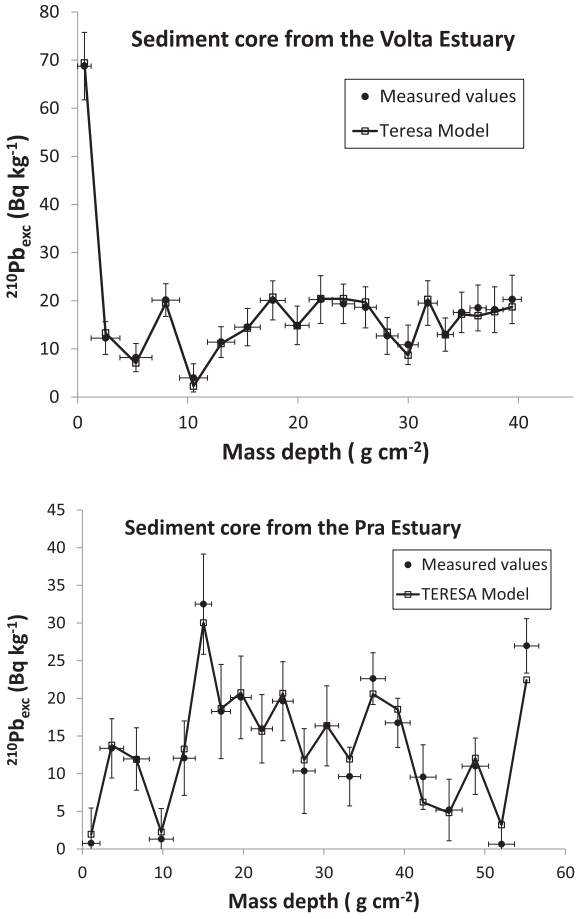

Fig. 5. $^{210}Pb_{exc}$ versus mass depth profile for the Volta and Pra cores. Vertical bars correspond to the associated uncertainties, while the horizontal ones define the mass depth interval of each sediment slice. The solutions generated by the TERESA model are plotted as points at the centre of each slice interval (continuous lines are only for guiding-eyes).

if physically meaningful, could be likely related to other poorly documented anthropogenic activities such as unauthorized sand winning or to recent engineering works at Ada-Foah area.

For the core from the Pra Estuary, the computed maps for the χ function (Fig. 6) show a well constrained minimum in the (s_A, s_w) space, while in the $(\overline{A}_0, \overline{w})$ space there is a well-defined valley in the region (20,4) and a narrow trench in the region of higher SAR values. The first one has been selected for generating the numerical solution. The computed $^{210}Pb_{exc}$ vs. mass depth profile is shown in Fig. 5 (panel 2), with the parameter values reported in Table 5. The resulting chronology is shown in Fig. 7. The age of the deepest layer is only 20.7 ± 0.5 y, which implies time-averaged SAR value of 2.73 ± 0.06 g cm^{-2}·y^{-1}. The slope of the chronological line is relatively uniform, and then the SAR value is almost constant, but two relative minima are found around 2000–2003 and 2007–2010. The overall higher SAR values found in the Pra Estuary, when compared against those from the Volta Estuary, are well consistent with its yearly discharge of about 1.14 Mt of suspended sediments (Akrasi and Ansa-Asare, 2008), this value is probably enhanced by the large concentration of gold mines in its basin. This situation is also reflected in the available aerial photographs (e.g., Google Earth, 07-06-2015) which show a huge cloud of suspended sediments being discharged by the Pra into the sea.

In the review-paper by Duarte et al. (2013), authors conducted a wide compilation of data from published literature for reporting accretion rates for three different classes of vegetated coastal sediments, namely salt marshes, mangroves and seagrasses. Higher values were found for salt marshes, being of 5.5 ± 0.7 mm y^{-1} (median and standard deviation from a set of 98 observations). The time-averaged values found from TERESA model for the studied 0–40 cm interval in the cores from the Volta and Pra estuaries were 10.4 ± 0.3 mm y^{-1} and 19.3 ± 0.5 mm y^{-1}, respectively. These values are noticeably higher than the above median, but still within the range 0.39–61.1 mm y^{-1} found by Duarte et al. (2013).

It is know that ^{210}Pb concentration profiles in sediments from dynamic environments such us estuarine and coastal areas, often exhibit intricate profiles which pose a great challenge to the usual dating models (e.g., Mahu et al., 2016; Serrano et al., 2016c). Most of the studies still use the assumption of a constant rate of supply, which hardly attains in these dynamical mass-flow dominated environments (see the two-component mass flow model with intrinsic scatter by Abril and Brunskill, 2014). Thus, according to results from TERESA model, the high values of the standard deviations in the entry parameters (Table 5) also imply a very high variability of the $^{210}Pb_{exc}$ fluxes onto the SWI, which had arithmetic mean and standard deviations of 580 ± 480 and 790 ± 680 Bq·m^{-2}·y^{-1} for the Volta and Pra estuaries, respectively.

Model misapplications can lead to inaccurate estimations of SAR and wrong interpretations of system dynamics and the history of anthropogenic impacts. Particularly, assessing the CO_2 sequestration potential of vegetated coastal ecosystems is a topic of increasing interest in recent years (e.g. see the review papers by Breithaupt et al., 2012; and by Xiaoguang Ouyang et al., 2017). For these studies, reliable estimations of burial rates at a centennial scale are of capital importance, what requires the use of ^{210}Pb-based dating models able to handle varying conditions for both, SAR and fluxes onto the SWI. The SIT model (Carroll and Lerche, 2003), which claimed its ability for handling these sedimentary conditions, lacks of a sound physical basis, as demonstrated by Abril (2015). The new TERESA model, based upon a widely observed statistical correlation between fluxes and SAR (Abril and Brunskill, 2014), can represent a reliable approach for these scenarios, but a wider set of application cases is necessary to better define its potentials and limitations.

4. conclusions

The measured specific activities for ^{234}Th, ^{226}Ra, ^{40}K, ^{228}Ra and ^{137}Cs in the cores from the Volta and Pra estuaries compared well with those reported by the scarce references found in the scientific literature for the studied areas. The specific activities of ^{210}Pb were similar to those found in other estuarine areas from Ghana and Morocco, but about 3–4 times lower than the ones reported for the Tema Harbor, in Ghana, this is likely due to the coarser granulometry of estuarine sediments. For ^{137}Cs, its specific activity was below the method detection limit in most of the cases.

The measured radionuclide concentrations do not pose any significant radioecological risk for the eleven species of organisms considered in the ERICA tool. Similarly, the five radiological indexes for human exposure (D, Ra_{eq}, H_{ex}, $AGDE$ and $AEDE$) and the estimated committed effective dose integrated for 50 years due to the ingestion of seafood were all well below the recommended limits.

While the assumptions for the application of conventional ^{210}Pb-based dating models were not meet, the new dating tool TERESA, which handles varying but correlated SAR and fluxes, was able to produce reliable chronologies for both studied cores. The ages of the deepest layers were of 38 ± 1 and 20.7 ± 0.5 y for the Volta and Pra estuaries, corresponding to time-averaged SAR values of 1.05 ± 003 and 2.73 ± 0.06 g cm^{-2}·y^{-1}, respectively. The core from the Volta reflects the sedimentary conditions prevailing after

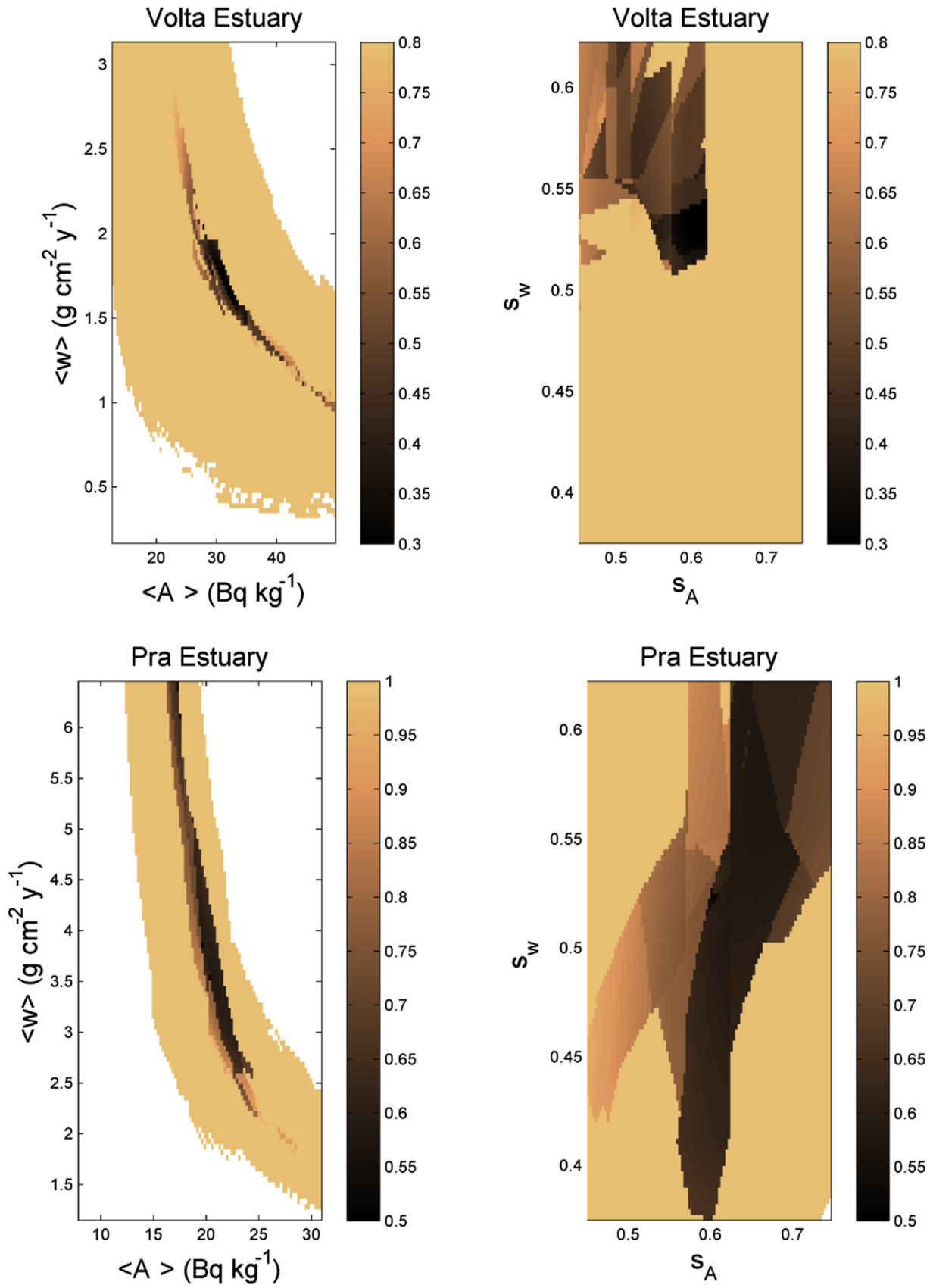

Fig. 6. Maps for the function χ computed by TERESA model for the cores from the Volta and Pra estuaries, and projected onto the planes (s_A, s_w) and ($\overline{A}_0$,$\overline{w}$) – this last written as (<A>, <w>). For each projection, the remaining parameter values are those corresponding to the minimum value of χ (see Table 5).

Table 5
Entry parameters and error estimates[a] for cores from the Volta and Pra estuaries.

Core	$\overline{A}_0$			$\overline{w}$			s_A			s_w			χ
Volta	34.6	±	0.2	1.63	±	0.01	0.52	±	0.03	0.56	±	0.01	0.29
Pra	19.40	±	0.06	3.90	±	0.04	0.606	±	0.006	0.522	±	0.006	0.51

[a] Through the second derivative of the Q^2 function (Bevington and Robinson, 2003).

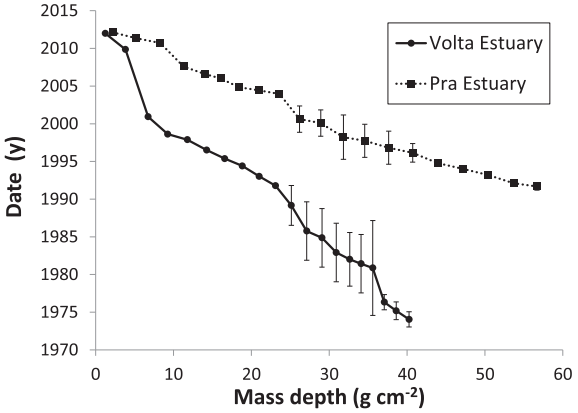

Fig. 7. Chronologies estimated by TERESA model for the cores from the Volta and Pra estuaries, along with their corresponding uncertainty intervals (from the propagation of error associated to the fitting parameters of Table 5).

the construction of the Akosombo Dam, and the higher SAR values found in the Pra are consistent with its huge discharge of suspended sediments enhanced by the intensive gold mining activities along its course.

Acknowledgements

The authors would like to extend gratitude to the International Atomic Energy Agency (IAEA) for supporting the Regional Project RAF7009 and the fellowship GHA-16025. Our appreciation also goes to the CNESTEN, in Morocco, where most of the analysis were carried out. Lastly many thanks to the staffs of the Marine and Fisheries Department of University of Ghana Legon and special thanks to Prof., B.J. B. Nyarko, Ghana Atomic Energy Commission (GAEC) for their supportive roles.

References

Abdi, M.R., Hassanzadeh, S., Kamali, M., Raji, H.R., 2009. ^{238}U, ^{232}Th, ^{40}K and ^{137}Cs activity concentrations along the southern coast of the Caspian Sea. Iran. Mar. Pollut. Bull. 58, 658–662.
Abril, J.M., 2003. A new theoretical treatment of compaction and the advective-diffusive processes in sediments. A reviewed basis for radiometric dating models. J. Paleolimnol. 30, 363–370.
Abril, J.M., 2011. Could bulk density profiles provide information on recent sedimentation rates? J. Paleolimnol. 46, 173–186.
Abril, J.M., 2015. Why would we use the Sediment Isotope Tomography (SIT) model to establish a ^{210}Pb-based chronology in recent-sediment cores? J. Environ. Radioact. 143, 40–46.
Abril, J.M., 2016. A ^{210}Pb-based chronological model for recent sediments with random entries of mass and activities: model development. J. Environ. Radioact. 151, 64–74.
Abril, J.M., Brunskill, G.J., 2014. Evidence that excess ^{210}Pb flux varies with sediment accumulation rate and implications for dating recent sediments. J. Paleolimnol. 52, 121–137.
Abril, J., Fraga, E., 1996. Some physical and chemical features of the variability of K_d distribution coefficients for radionuclides. J. Environ. Radioact. 30 (3), 253–270.
Adjei-Boateng, D., Agbo, N.W., Agbeko, N.A., Obirikorang, K.A., Amisah, S., 2012. The current state of the clam, *Galatea paradoxa*, fishery at the Lower Volta River, Ghana. In: IIFET Tanzania Proceedings.
Akrasi, S.A., Ansa-Asare, O.D., 2008. Assessing sediment and nutrient transport on the Pra basin of Ghana. West Afr. J. Appl. Ecol. 13, 61–71.
Allen, G.P., Salmon, J.C., Bassoullet, P., Penhoat, Y., De Grandpre, C., 1980. Effect of tides on mixing and suspended sediment transportation in macrotidal estuaries. Sedim. Geol. 26, 69–90.
Amekudzie, A., Emi-Reynolds, G., Faanu, A., Darko, E., Awudu, A., Adukpo, O., Quaye, L.A.N., Kpordzro, R., Agyemang, B., Ibrahim, A., 2011. Natural radioactivity concentrations and dose assessment in shore sediments along the coast of Greater Accra, Ghana. World Appl. Sci. J. 13 (11), 2338–2343.
Appleby, P.G., 2008. Three decades of dating recent sediments by fallout radionuclides: a review. Holocene 18, 83–93.
Bevington, P.A., Robinson, D.K., 2003. Data Reduction and Error Analysis for the Physical Sciences, third ed. McGraw-Hill, New York.
Botwe, B.O., Schirone, A., Delbono, I., Barsanti, M., Delfanti, R., Kelderman, P., Nyarko, E., Lens, P.N.L., 2017. Radioactivity concentrations and their radiological significance in sediments of the Tema Harbour (Greater Accra, Ghana). J. Radiat. Res. Appl. Sci. 10, 63–71.
Breithaupt, J.L., Smoak, J.M., Smith, T.J., Sanders, C.J., Hoare, A., 2012. Organic carbon burial rates in mangrove sediments: strengthening the global budget. Glob. Biogeochem. Cycles 26 (3).
Brown, J.E., Alfonso, B., Avila, R., Beresford, N.A., Copplestone, D., Prohl, G., Ulanovsky, A., 2008. The ERICA tool. J. Environ. Radioact. 99, 1371–1383.
Brown, J.E., Alfonso, B., Avila, R., Beresford, N.A., Copplestone, D., Hosseini, A., 2016. A new version of the ERICA tool to facilitate impact assessment of radioactivity on wild plants and animals. J. Environ. Radioact. 153, 141–148.
Carroll, J., Lerche, I., 2003. Sedimentary Processes: Quantification Using Radionuclides. Elsevier, Oxford.
Duarte, C.M., Losada, I.J., Hendriks, I.E., Mazarrasa, I., Marbà, N., 2013. The role of coastal plant communities for climate change mitigation and adaptation. Nat. Publ. Gr 3, 961–968.
El Mamoney, M., Khater, A.E., 2004. Environmental characterization and radioecological impacts of non-nuclear industries on the Red Sea coast. J. Environ. Radioact. 73, 151–168.
Fisher, N.S., Beaugelin-Seiller, K., Hinton, T.G., Baumann, Z., Madigan, D.J., Garnier-Laplace, J., 2013. Evaluation of radiation doses and associated risk from human consumers of seafood. PNAS 110, 26 pnas.org/cgi/doi/10.1073/pnas.1221834110.
Goldberg, E.D., 1963. In: Geochronology with Pb-210. Proceedings of a Symposium of Radioactive Dating. International Atomic Energy Agency, Vienna, pp. 121–131.
ICRP, 2008. Environmental Protection: the concept and use of reference animals and plants. ICRP publication. Ann. ICRP 38 (108), 4–6.
Keller, Th, Häkansson, I., 2010. Estimation of reference bulk density from soil particle size distribution and soil organic matter content. Geoderma 154, 398–406.
Koide, M., Soutar, A., Goldberg, E.D., 1972. Marine geochronology with ^{210}Pb. Earth Planet. Sci. Lett. 14, 442–446.
Kpeglo, D., Mantero, J., Darko, E., Emi-Reynolds, G., Faanu, A., Manjón, G., Vioque, I., Akaho, E.H.K., García-Tenorio, R., 2016. Radiochemical characterization of produced water from two production offshore oilfields in Ghana. J. Environ. Radioact. 152, 35–45.
Krishnaswamy, S., Lal, D., Martin, J.M., Meybek, M., 1971. Geochronology of lake sediments. Earth Planet. Sci. Lett. 11, 407–414.
Kurnaz, A., Kucukomeroglu, B., Keser, R., Okumusoglu, N., Korkmaz, E., Karahan, D., Çevik, U., 2006. Determination of radioactivity levels and hazards of soil and sediment samples in Firtina Valley (Rize, Turkey). Appl. Radiat. Isot. 65, 1281–1289.
Laissaoui, A., Mas, J.L., Hurtado, S., Ziad, N., Villa, M., Benmansour, M., 2013. Radionuclide activities and metal concentrations in sediments of the Sebou Estuary, NW Morocco, following a flooding event. Environ. Monit. Assess. 185, 5019–5029.
Larsson, C.M., 2008. An overview of the ERICA Integrated Approach to the assessment and management of environmental risks from ionising contaminants. J. Environ. Radioact. 99 (9), 1364–1370.
Lick, W., Huang, H., 1993. Flocculation and the physical properties of flocs. In: Mehta, A.J. (Ed.), Nearshore and Estuarine Cohesive Sediment Transport. American Geophysical Union, Washington, DC, pp. 21–39.
Ly, C.K., 1980. The role of the Akosombo Dam on the Volta River in causing coastal erosion in central and eastern Ghana (West Africa). Mar. Geol. 37 (3–4), 323–332.
Mabit, L., Benmansour, M., Abril, J.M., Walling, D.E., Meusburger, K., Iurian, A.R., Bernard, C., Tarján, S., Owens, P.N., Blake, W.H., Alewell, C., 2014. Fallout ^{210}Pb as

a soil and sediment tracer in catchment sediment budget investigations: a review. Earth-Sci. Rev. 138, 335–351.
Mahu, E., 2014. Geochemistry of Estuarine Sediments of Ghana: Provenance, Trace Metal Accumulation Trends and Ecotoxicological Risks. Ph.D. Thesis. University of Ghana.
Mahu, E., Nyarko, E., Hulme, S., Swarzenski, P., Asiedu, D.K., Coale, K.H., 2016. Geochronology and historical deposition of trace metals in three tropical estuaries in the Gulf of Guinea. Estuar. Coas. Shelf S 177, 31–40.
Morton, R.A., 2003. An overview of coastal land loss: with emphasis on the Southeastern United States. USGS OFR 03–337.
Nichols, M.M., Johnson, G.H., Peebles, P.C., 1991. Modern sediment and facies model for a macrotidal plain estuary and the James Estuary, Virginia. J. Sedim. Petrol 61, 883–899.
Nyarko, E., Botwe, B., Ansong, J., Delfanti, R., Barsanti, M., Schirone, A., Delbono, I., 2011. Determination of ^{210}Pb, ^{226}Ra and ^{137}Cs in beach sands along the coastline of Ghana. Afr. J. Environ. Pollut. Health 9, 17–23.
Postma, H., 1967. Sediment transport and sedimentation in the estuarine environment. In: Lauf, G.H. (Ed.), Estuaries. America Association for the Advancement of Science, Washington, DC, pp. 158–179.
Robbins, J.A., 1978. Geochemical and Geophysical applications of radioactive lead isotopes. In: Nriago, J.P. (Ed.), Biochemistry of Lead in the Environment. Elsevier, Amsterdam, pp. 285–393.
Rurangwa, E., Agyakwah, S.K., Boon, H., Bolma, B.C., 2015. Development of Agricultural in Ghana Analysis of the Fish Value Chain and Potential Business Case. IMARES report C021/15.
Sánchez-Cabeza, J.A., Ruíz-Fernández, A.C., 2012. ^{210}Pb sediment radiochronology: an integrated formulation and classification of dating models. Geochim. Cosmochim. Act. 82, 183–200.
Schmid, E., Schrader, T., 2007. Different biological effectiveness of ionising and non-ionising radiation in mammalian cells. Adv. Radio Sci. 5, 1–4.
Serrano, O., Ruhon, R., Lavery, P.S., Kendrick, G.A., Hickey, S., Masqué, P., Arias-Ortiz, A., Steven, A., Duarte, C.M., 2016c. Impact of mooring activities on carbon stocks in seagrass meadows. Sci. Rep. 6, 23193.
Tanner, T., Mensah, A., Lawson, E.T., Gordon, C., Godfrey-Wood, R., Cannon, T., 2014. Political Economy of Climate Compatible Development: Artisanal Fisheries and Climate Change in Ghana. IDS working paper 446.
UNSCEAR, 2000. In: Sources and Effects of Ionizing Radiation: Sources, vol. 1. United Nations Publications, New York.
UNSCEAR, 2008. In: Sources and Effects of Ionizing Radiations, vol. 1. United Nations Publications, New York.
Velinsky, D., Sommerfiled, C., Enache, M., Charlse, D., 2011. Final Report, Nutrient and Ecological Histories in Barnegat Bay, New Jersey. Patrick Center for Environmental Research. The Academy of Natural Sciences, Philadelphia, PA, p. 19103.
Woodruff, J.D., Geyer, W.R., Sommerfield, C.K., Driscoll, N.W., 2001. Seasonal variation of sediment deposition in the Hudson River estuary. Mar. Geol. 179, 105–119.
Xiaoguang Ouyang, X., Lee, S.Y., Connolly, R.M., 2017. The role of root decomposition in global mangrove and saltmarsh carbon budgets. Earth-Sci. Rev. 166, 53–63.
Xinwei, L., Lingqing, W., Xiaodan, J., 2006. Radiometric analysis of Chinese commercial granites. J. Radioanal. Nucl. Ch. 267, 669–673.